Development of in-flow label-free single molecule sensors using planar solid-state nanopore integrated microfluidic devices

Fatma D. Güzel[1,2] ✉, *Benjamin Miles*[2]

[1]*Biomedical Engineering, Ankara Yildirim Beyazit University, 06010 Etlik/Ankara, Turkey*
[2]*Department of Chemistry, Imperial College London, South Kensington Campus, London, SW7 2AZ, UK*
✉ *E-mail: fdogan@ybu.edu.tr*

Published in Micro & Nano Letters; Received on 28th February 2018; Revised on 22nd May 2018; Accepted on 8th June 2018

Nanopore biosensors have attracted attention due to their label-free single molecule detection capability. To date, different materials and applications have been shown in the field, varying from Si_3N_4 to graphene and biomolecule sensing to DNA sequencing. Classical nanopore devices are composed of Si_3N_4 material supported on a Si wafer and the detection is largely based on electrochemical sensing using chambers of ml volumes on both sides of the nanopore device. In this study, in-flow label-free electrochemical detection of DNA molecules at single molecule level is shown using a classical Si_3N_4 nanopore device integrated into a microfluidic device. The layout of the device given here set the basics for future works and discussions regarding future microfluidic integrated solid-state nanopores and the behaviour of the molecule under the influence of hydrodynamic flow.

1. Introduction: In the recent decade, the field of biosensors has been growing fast, clearly in response to increasing clinical demands towards a better understanding of the biological mechanisms as well as the use of easy-to-perform, cheap and highly efficient assays. Among many types of biosensors developed so far [1–7], nanopores hold great promise as biosensors with single molecule detection capability, whether naked or functionalised, electrochemical or optical [8, 9]. A nanopore is either formed biologically on a lipid bilayer or engineered on an insulating nanoscale material using semiconductor technology. The layer that a single nanopore is constituted on is called '*membrane*' in either case. The membrane separates two chambers in an ionic solution and the pore provides an ionic pathway between each chamber. Upon the application of an electric field across the nanopore, a stable ionic current trace is observed due to the passage of the electrolyte ions. Once any molecule larger the electrolyte ions in size is added to one of the compartments, the molecule is forced to pass through the nanopore while blocking the pore for a certain amount of time. This also means the blockage of the ionic current, recorded as modulations of the current trace. Each current modulation provides detailed information about the charge, conformation and size of the molecule inside the pore.

Different nanopore materials have already been shown extensively [8, 10–13]. The future of nanopores arguably lies in their integration with other platforms such as microfluidic networks in order to provide automation and ease in handling the liquid exchange. There are a few examples published recently, which illustrate the combination of several different types of solid-state nanopore chips with microfluidic channels, applied for various applications [14–24]. For example, several groups showed the integration of a membrane with an array of nanopores for the study of bacterial samples and size selective DNA transport based on monitoring the capture optically [14, 15, 18]. Integration of single nanopores in the microfluidic channels has also been reported recently that used different materials and device fabrication techniques for several applications like the translocation of ribosomal subunits and DNA [17, 19, 25, 26]. A single-capillary integrated microfluidic device has also been shown for the label-free in-flow detection of single DNA molecules [27]. In a similar attempt, Timp and co-workers [20] showed the use of classical single silicon nitride (Si_3N_4) nanopore integrated device for the study of individual cells. Nanopore-integrated microfluidic devices seem to attract the interest of biosensor researchers, however, in the previous studies either nanopore arrays were used or the fabrication of the nanopore device was too demanding or detection was not performed under continuous flow. To the best of our knowledge, there has not been any study that proved the electrochemical detection of single biomolecules under continuous flow conditions using the classical single Si_3N_4 nanopore-integrated device and fabrication techniques. This is rather important because of the familiarity of the nanopore researchers with the process and also, more importantly, the potential of such a hybrid device for the label-free in-flow electrochemical detection of analytes using commonly known nanopore devices. The employment of continuous flow is a prerequisite for the functionality of microfluidic channels on a lab-on-chip device. By achieving this, one can construct a monolithic device that enables the detection of single species while being simultaneously processed (e.g. sample purification, separation, and amplification if necessary). Also, the in-flow electrochemical detection circumvents the need for labelling of the molecules as in most of the in-flow optical-based single molecule sensors [28].

The working principle of the planned device is as follows: DNA sample prepared in an electrolyte solution is infused through the microfluidic channel, as illustrated in Fig. 1. Electrodes are inserted into the corresponding electrolyte chambers; one is at the outlet of the microfluidic channel (cis), the other is at the back side of the chip (trans). Once a certain voltage is applied across the membrane, the electric field generated across the pore forces DNA to transverse to the other side of the nanopore from the inset of the microfluidic channel, whether it be in the absence or in the presence of flow. We believe the demonstration of the step-by-step construction of the hybrid device and the treatment of the electrochemical nanopore detection in conjunction with the flow dynamics shown here constitutes the basics for future forms of the nanopore integrated microfluidic sensing.

2. Experimental section

2.1. Fabrication: Fabrication of the device comprises three steps: Fabrication of nanopore chip, fabrication of microfluidic chip and their integration. The schematic diagram and an image of the hybrid device are shown in Fig. 2 (left and right, respectively). Though classical semiconductor processing techniques were used to fabricate Si_3N_4 nanopore devices, as presented earlier by Ayub

doi: 10.1049/mnl.2018.5206

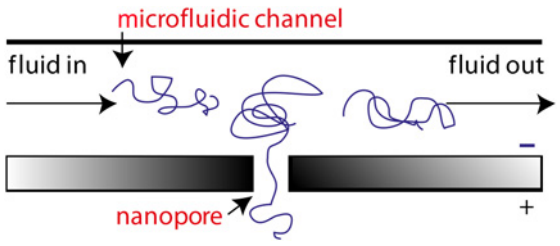

Fig. 1 *Schematic diagram of the single nanopore integrated the microfluidic chip*

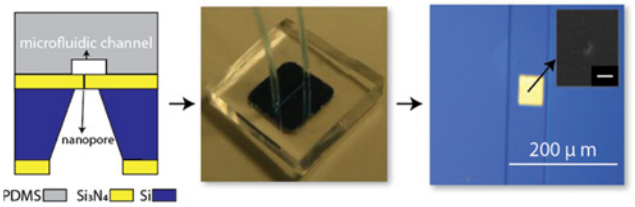

Fig. 2 *Left: Schematic diagram of the integrated chip. Middle image: Photograph of the chip. Right image: Optical image of the microfluidic channel aligned to the free-standing Si_3N_4 window. Inlet: An example SEM image of a nanopore. Scale bar is 200 nm*

et al. [20], the design of the chip differs slightly in order to conform to the integration process. Free-standing Si_3N_4 nanopore devices supported on a micron thick ⟨100⟩ silicon (Si) substrate are 10×10 mm in size in order to support the integration into the microfluidic system-unlike the common device size of 5×5 mm. The layout for the photomask was drawn in KLayout drawing software and AutoCad Civil 3D. Acetate mask was produced by Micro Lithography Services Ltd (UK). The initial Si_3N_4 window size of 444×444 µm resulted in 50×50 µm wide free standing Si_3N_4 windows at the centre of each individual chip after potassium hydroxide (KOH) etch. Focused Ion Beam (FIB) parameters were 30 kV acceleration voltage and 1 pA beam current. A milling time of 6 s, corresponding to a dose of $2^{-5} \times 10^{22}$ coulomb per metre square (C/m^2) was used to drill nanopores producing open pores varying from 20 to 60 nm in the diameter.

Microfluidic chips made of polydimethylsiloxane (PDMS) were fabricated using classical soft and photolithography methods [21]. The entire PDMS chip is 25×25 mm in size. Microchannel dimensions are 6 mm × 75 µm × 75 µm (length, width, depth, respectively), and results in <50 psi pressure drop across the channel for flow rates smaller than 0.3 µl/min. The length of the channel and the pressure drop across are well-suited for the integration with nanopore device. Once aligned with the nanopore device, the entire channel network operates on the surface of the nanopore device. This prevents a potential leakage between two devices when the fluid is pumped through the channels. The centre of tubing connections is designed to be 2 mm away from the edges of the nanopore device. Also, the microfluidic channel width is larger than the size of the free-standing Si_3N_4 window because the PDMS bonding would damage the nanometre-thick membrane if directly bonded on the window. The alignment is shown in the right image in Fig. 2. To assist the positioning of the PDMS chip onto the nanopore device and the finer alignment of the channel onto the Si_3N_4 window, particular markers are added to the microfluidic design and the gap between the edges of each marker and the channel is around 275 µm.

Integration was achieved by plasma treatment of the surfaces and bringing the chips into contact straight afterwards. The integration process is described below: 1 mm holes were opened up in PDMS chip using a 1 mm punch and it was sonicated in ethanol for 20 min, followed by isopropanol and water treatment for 5 min, drying with nitrogen (N_2) blow. Nanopore chips were treated with piranha solution. Both chips – microchannel side of the PDMS chip and free-standing Si_3N_4 layer side of the nanopore chip – were then exposed to oxygen plasma (Harrick Plasma, USA) for about 70 s. The chips were brought into contact under a stereomicroscope straight after the plasma treatment (within 20 s). To do so, the Si_3N_4 chip was first fixed under the optics using an adhesive film (Gel-Pak, UK) and PDMS chip was aligned onto the nanopore chip quickly. After carefully removing the chip from the adhesive surface, the chip was placed on a hot plate at 80°C for a couple of hours.

Fig. 2 presents a schematic diagram of the integrated chip and a photograph of the actual device (left and the middle, respectively) as well as an optical image of an example chip aligned (right), where a 73 ± 2 µm wide microfluidic channel was integrated onto a 50×50 µm free-standing Si_3N_4 window (yellow square) with a nanopore. An example SEM image of a nanopore ($d_{pore} = 23 \pm 5$ nm) is shown in the far-right figure. The success rate of alignment is sufficiently high, providing that the surface of each chip is clean, smooth and hydrophilic enough, while the alignment is carried out sufficiently fast before the surface deactivation.

2.2. Electrochemical characterisation: Potassium chloride (KCl) solution (VWR, UK) was prepared in 10 mM Tris hydrochloride (Tris HCl) and 1 mM ethylenediaminetetraacetic acid (EDTA) buffered at pH = 8 (Sigma-Aldrich, UK), autoclaved and filtered (Pall Corporation, UK, pore size: 200 nm). Silver/silver chloride (Ag/AgCl) electrodes were prepared by coating 0.25 mm Ag wire surface (GoodFellow, UK) with a solid thin layer of AgCl, stored dry or in KCl solution in the dark. Simply, Ag wire is chloridised in 2 M HCl (Chronopotentiometry, current: 0.01 mA, voltage: 6 V and time: 900 s). The back side of the integrated device – nanopore open side – was exposed to oxygen (O_2) plasma for at least 5 min and wetted with ethanol and distilled (deionised water – DI) water afterwards. The electrolyte solution was then infused into the microfluidic channel after the tubing of the syringe was inserted into the inlet opening of the PDMS chip. The chip was tightly sealed between two polymeric cell reservoirs, where the edges of the Si_3N_4 chip in the trans reservoir were protected precisely in order to eliminate any noise contribution to the current signal. The volume of the chambers is 1 ml while the sample volume of the microfluidic channel is about 1 nl. Prior to each experiment, the electrolyte solution was flushed through the channel for at least 10 min at 1–5 µl/min flow rates and then both reservoirs were rinsed with DI water followed by the electrolyte so that any residual particles either inside the channel or outside was removed.

The apparatus was placed in a Faraday cage on an anti-vibration table. Syringe tubing connection between the pump (Harvard Apparatus, UK) and the chip was also wrapped in aluminium foil tightly to minimise the noise. Preliminary ionic current measurements were performed using Gamry Reference 600 potenstiostat (Gamry Instruments, USA) whereas the translocation experiments were carried out using a patch clamp amplifier (Axopatch 200B, Molecular Devices, USA). Data was acquired using an electrophysiology data acquisition and analysis software (pCLAMP^{tm}, Molecular Devices, USA), sampled at 50 kHz, filtered at 2–5 kHz using a 4-pole low-pass Bessel filter, and digitised using an A/D convertor (Digidata® 1550 Data Acquisition System, Molecular Devices, USA). Data analysis was performed using Clampfit 10.2 (Molecular Devices, USA) and a particular Matlab code.

3. Results and discussion: We first studied the effect of flow in conductance, G, open pore current, I_o, and the nanopore noise at a variety of flow rates ranging from 0.02 to 5 µl/min. Between each experiment, there was a waiting time of 10 min. Conductance and pore diameter were calculated using the nanopore conductance equation [12]. Second, it was shown that

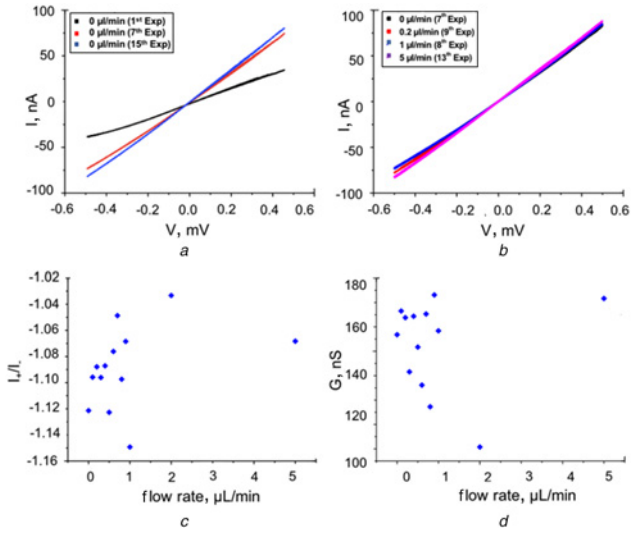

Fig. 3 *Electrochemical characterisation of the integrated chip*
a *I–V* curves recorded at 0 flow rate at different recording times
b *I–V* curve recorded at different flow rates; 0, 0.2, 1 and 5 µl/min (Experimental order; 7th, 9th, 8th, 13th, respectively)
c Current rectification extracted from each *I–V* curve recorded at different flow rates
d Nanopore conductance extracted from each *I–V* curve recorded at different flow rates (1 M KCl, 10 mM Tris HCl and 1 mM EDTA)

the performance of the integrated chip is compatible with current nanopore devices both in the absence and presence of flow. Finally, the effect of flow on DNA translocation statistics was discussed based on the experimental findings.

In Fig. 3, some of the *I–V* curves obtained in the absence of flow (Fig. 3*a*), using different flow rates (Fig. 3*b*), ionic rectification and conductance versus flow rates (Figs. 3*c* and *d*, respectively) are plotted. A drastic change in the conductance (48%) was observed when comparing the initial and final *G* while the change dropped down to 6% towards the end of the experiments. The direct interpretation of this result is that the system supposedly reached an equilibrium state over time. This can be better understood from d_{exp}, which enlarged from an initial diameter of 27 to 39 nm at the end. One hypothesis for this change is that the nanopore was initially partially blocked due to insufficient wetting of the nanopore surface and applying a voltage across the nanopore assisted in improving the wetting properties [29]. Instability due to the surface properties of the nanopore modified by the ion beam irradiation is perhaps another reason. The order of the experiments at different flow rates were not kept in order so as to observe the effect of experiment duration in the results. It was observed that the *G* kept increasing although the flow rate was lowered (i.e. changing the flow rate from 0 to 1 µl/min and then 0.2 µl/min). This means that the change in G_{exp} is related to the change in nanopore diameter over time and not the increase in the flow rate. Repeat experiments also proved this; as a result, it was concluded that the effect of flow to the ionic current was not of a significant magnitude.

The next step was to ascertain if there is any ionic current-rectification, which is, in general, a consequence of asymmetric ion transport due to surface charge discontinuities or asymmetric pore geometries [30]. In our experiments, this might be observable due to the flow stream on one side of the nanopore. To reveal the effect, the rectification ratio (ratio of the current with different polarities, I_+/I_-) was investigated. The results are shown in Fig. 3*c*. It was observed that I_+/I_- does not show any substantial trend and can be interpreted that the flow through the nanopore was also negligible at the chosen flow rates for such an effect in the ionic current. RMS noise with respect to the flow rate was also investigated preliminarily. Results indicated a variation in the order of <10 pA in RMS noise.

For translocation experiments, a stable open pore current was first established at different voltages before the addition of DNA. In the second step, DNA (1 or 10 µl of 500 ng/µl λ-DNA, corresponding to 15.5 nM or 155 nM, respectively) diluted in 1 M KCl, 10 mM Tris HCl and 1 mM EDTA buffer, was pumped into the microfluidic channel and each measurement was taken after at least 2 min of pumping at the following flow rate in order to reach an equilibrium state between different flow rates. The most compelling evidence for a translocation event/current blockade in a current-time trace is that translocation type signals appear at high voltages and the amplitude of the current blockade enhances with the increase in voltage applied. To confirm the compatibility of the device with commonly used nanopore devices, the voltage dependency of the current blockades was examined. At low voltages (i.e. 50 mV) there was no current blockade observed. When the voltage was increased to a higher level (i.e. 100 mV and above) there was a clear indication that the translocation types current blockades with an increase in signal-to-noise ratio appeared, in good agreement with the literature [31]. It was, therefore, assumed that these were the consequences of the DNA translocation. As a proof-of-concept, the translocation of DNA in flow was studied using a nanopore with a diameter of 12–21 nm on a 100 nm thick Si_3N_4 membrane. Fig. 4*c* presents 1.5 s current–time trace recorded at a flow rate of 2 µl/min. Under flow conditions, there was not any observable trend between the translocation frequency, *f*, and the flow rates, statistics changing from experiment to experiment.

In flow, the molecules are in fact forced to conform to flow through the microfluidic channel, as illustrated in Fig. 4*a*. An accurate representation of the DNA capture process in flow requires further consideration of coupling of its diffusive, electrostatic and hydrodynamic velocity components (e.g. the diffusion velocity, the drift velocity and the fluid velocity profiles) in three dimensions (3D), leading to a discussion on different regimes affecting the molecule behaviour: diffusion-limited regime, transitional regime and flow-limited regime.

In the diffusion-limited regime, DNA capture is only affected by the diffusive flux in all directions and the fluid flow contribution in the *x*-direction. Whereas in the energy barrier-limited regime, convective forces are dominantly active, which themselves are influenced by the molecular transport in the *z*-direction due to electrophoretic forces, and the fluid flow in the *x*-direction. It is explicit that the capture can no longer be described by the aforementioned regimes with no consideration to flow but requires additional consideration of the superposition of the diffusion and convective fluxes in 3D. At low flow rates, the classic theory of capture rate can still be applied. However, at high flow rates, the effect of the diffusive flux should be eliminated because the molecular motion is streamlined by the increase in the convective forces in the *x*-direction. In addition, an intermediate level where the interplay between diffusive and convective forces occurs is also feasible at medium flow rates. Furthermore, DNA loses its relaxed state under a certain degree of stress. It is therefore considered that there is a need for a physical description of the capture phenomena in flow covering all the velocity components, DNA conformational changes and time dependent variables such as relaxation time of the molecule; the diffusion-limited regime, transitional regime from diffusion-limited to flow-limited regimes and flow-limited regime.

- *Diffusion-limited regime:* Flow velocity is relatively small compared to drift velocity, meaning that the traditional nanopore capture concept is valid [32, 33].

- *Transitional regime:* Flow velocity becomes comparable to drift velocity. In this regime, the presumption is that a force balance between diffusive forces and convective forces governs DNA translocation. In terms of DNA conformation, the flow starts to impose a hydrodynamic force on the molecule where DNA is not flexibly

doi: 10.1049/mnl.2018.5206

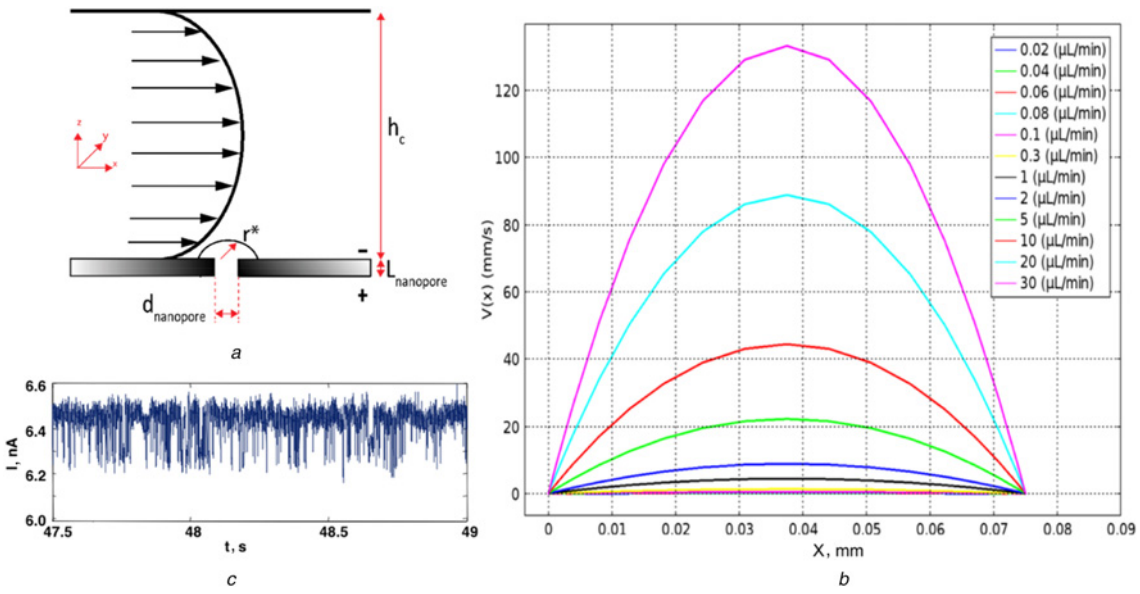

Fig. 4 *Schematic representations of flow profile in the microfluidic channel and in-flow examination of DNA translocation*
a Schematic diagram of the DNA capture through a nanopore embedded into a microfluidic channel in flow
b Flow velocity profile in a 75 µm × 75 µm × 6 mm microchannel, simulated using COMSOL Multiphysics®. Flow rates: 0.02, 0.04, 0.06, 0.08, 0.1, 0.3, 1, 2, 5, 10, 20, 30 µl/min
c Example of 1.5 s current–time traces recorded at 250 mV at a flow rate of 2 µl/min (d_{exp} = 12–21 nm, L_{SiN} = 100 nm. 15. 5 pM DNA in 1 M KCl, 10 mM Tris HCl and 1 mM EDTA)

coiled up anymore and is partially coiled up. The degree of coiling and elongation can only be studied theoretically or using high-resolution optical instrumentation experimentally.

• *Flow-limited regime:* Flow velocity is relatively large in comparison to drift velocity. This means that the molecule travels along the *x*-axis faster than its potential travel in the *z*-axis towards the nanopore. Perhaps there are two sub-regimes for the flow-limited regime; one is that translocation still occurs, but translocation time and velocity are rather manipulated by the flow velocity and degree of DNA elongation and the other is where translocation stops due to the high speed of the molecule in the *x*-direction.

In a planar nanopore-integrated microfluidic device like Si_3N_4/PDMS integration, the treatment of these regimes is not straight-forward due to the parabolic velocity profile of flow with no-slip boundary conditions and the nanoscale dimension of the nanopore capture zone. Calculating the velocity gradient across the channel using the Hagen–Poiseuille equation, one finds that the flow velocity around the nanopore capture zone clearly becomes negligible at low flow rates (e.g. 2 µl/min and less, $V(x) < 2$ mm/s) [34]. The effective nanopore capture distance and the drift velocity at the nanopore entrance are $r^* < 500$ nm and 94 mm/s for 20 nm wide, 100 nm thick nanopore, respectively ($\mu_{\lambda\text{-DNA}} = 3.73 \times 10^{-4}$ cm^2/Vs) and thus the flow velocity around the capture zone clearly becomes negligible at low flow rates (e.g. 2 µl/min and less, $V(x) < 2$ mm/s) [35]. A simulation for a non-compressible, Newtonian, laminar fluid flow was run using COMSOL Multiphysics® so that the velocity gradient across the channel in this system could be visualised, as shown in Fig. 4*b*. The consequent flow profile at different flow rates ranging from 0.02 to 30 µm/min indicates that an effective flow gradient through the nanopore can only form at high flow rates because of the occurrence of relatively low flow velocity near the wall. This would potentially alter the dynamics of the translocation process and thus the effect requires to be taken into account when working with higher flow velocities than the experimented flow rates. An additional discussion is presented in Appendices 1 and 2.

4. Conclusion: The work presented here aims to set out a roadmap for the development of a compact nanopore sensing device integrated into a microfluidic chip. The capability of in-flow single molecule detection based on electrochemical identification is also shown as a proof-of-concept, which is a label-free alternative to optical based in-flow single molecule experiments. It also opens up a discussion for the nanopore capture behaviour of DNA in flow on planar nanopore integrated devices, as opposed to the previously presented discussion with the capillary integrated microfluidic device where the tip of the capillary, that is the nanopore, is presumably located in the centre of the channel and affected by the flow profile directly [27]. Different capture regimes of DNA in flow, as opposed to the classic nanopore capture theory, can be given as; the diffusion-limited regime, transitional regime, and flow-limited regime. Although it is still at a preliminary stage, the findings set the basics for the future microfluidic integrated planar nanopore applications (e.g. on-nanopore chip CE or on-nanopore chip PCR) and are therefore of great importance to the field. The flow rates chosen here are compatible with chip-based pre-analytical and biological processing techniques, where the flow rate is kept at a reasonable level. Awareness of the challenges and the working conditions of nanopores in flow when planer nanopore devices are used would, therefore, provide a significant ease to the development of more sophisticated on-nanopore integrated devices.

5. Acknowledgments: The authors thank Joshua B. Edel and Tim Albrecht for their stimulating discussions. This work was supported by the Turkish Ministry of Education.

6 References

[1] Misawa N., Osaki T., Takeuchi S.: 'Membrane protein-based biosensors', *J. R. Soc. Interface*, 2018, **15**, (141), doi: 10.1098/rsif.2017.0952
[2] Bhalla N., Di Lorenzo M., Pula G., *ET AL.*: 'Protein phosphorylation analysis based on proton release detection: potential tools for drug discovery', *Biosens. Bioelectron.*, 2014, **54**, pp. 109–114
[3] Bhalla N., Di Lorenzo M., Pula G., *ET AL.*: 'Protein phosphorylation detection using dual-mode field-effect devices and nanoplasmonic sensors', *Sci. Rep.*, 2015, **5**, p. 8687

[4] Bhalla N., Sathish S., Galvin C.J., *ET AL.*: 'Plasma-assisted large-scale nanoassembly of metal–insulator bioplasmonic mushrooms', *ACS Appl. Mater. Interfaces*, 2018, **10**, (1), pp. 219–226
[5] Bahadir E.B., Sezginturk M.K.: 'Applications of commercial biosensors in clinical, food, environmental, and biothreat/biowarfare analyses', *Anal. Biochem.*, 2015, **478**, pp. 107–120
[6] Avci H., Dogan Guzel F., Erol S., *ET AL.*: 'Recent advances in organ-on-a-chip technologies and future challenges: a review', *Turkish J. Chem.*, 2018, **42**, (3), pp. 587–610
[7] Mehrotra P.: 'Biosensors and their applications – a review', *J. Oral Biol. Craniofacial Res.*, 2016, **6**, (2), pp. 153–159
[8] Miles B.N., Ivanov A.P., Wilson K.A., *ET AL.*: 'Single molecule sensing with solid-state nanopores: novel materials, methods, and applications', *Chem. Soc. Rev.*, 2013, **42**, (1), pp. 15–28
[9] Gooding J.J., Gaus K.: 'Single-molecule sensors: challenges and opportunities for quantitative analysis', *Angew. Chem. Int. Ed. Engl.*, 2016, **55**, (38), pp. 11354–11366
[10] Howorka S.: 'Building membrane nanopores', *Nat. Nanotechnol.*, 2017, **12**, (7), pp. 619–630
[11] Bell N.A.W., Keyser U.F.: 'Nanopores formed by DNA origami: a review', *FEBS Lett.*, 2014, **588**, (19), pp. 3564–3570
[12] Guzel F.D., Avci H.: 'Fabrication of nanopores in an ultra-thin polyimide membrane for biomolecule sensing', *IEEE Sens. J.*, 2018, **PP**, (99), p. 1
[13] Stoloff D.H., Wanunu M.: 'Recent trends in nanopores for biotechnology', *Curr. Opin. Biotechnol.*, 2013, **24**, (4), pp. 699–704
[14] Kovarik M.L., Jacobson S.C.: 'Integrated nanopore/microchannel devices for ac electrokinetic trapping of particles', *Anal. Chem.*, 2008, **80**, (3), pp. 657–664
[15] Sheng Y., Bowser M.T.: 'Size selective DNA transport through a nanoporous membrane in a PDMS microfluidic device', *Analyst*, 2012, **137**, (5), pp. 1144–1151
[16] Rudenko M.I., Yin D., Holmes M., *ET AL.*: 'Integration and characterization of SiN nanopores for single-molecule detection in liquid-core ARROW waveguides', Proc. SPIE 6444, Ultrasensitive and Single-Molecule Detection Technologies II, San Jose, CA, 2007, p. 64440L
[17] Jain T., Guerrero R.J.S., Aguilar C.A., *ET AL.*: 'Integration of solid-state nanopores in microfluidic networks via transfer printing of suspended membranes', *Anal. Chem.*, 2013, **85**, (8), pp. 3871–3878
[18] Guo P., Hall E.W., Schirhagl R., *ET AL.*: 'Microfluidic capture and release of bacteria in a conical nanopore array', *Lab Chip*, 2012, **12**, (3), pp. 558–561
[19] King T.L., Gatimu E.N., Bohn P.W.: 'Single nanopore transport of synthetic and biological polyelectrolytes in three-dimensional hybrid microfluidic/nanofluidic devices', *Biomicrofluidics*, 2009, **3**, (1), p. 12004
[20] Ayub M., Ivanov A., Hong J., *ET AL.*: 'Precise electrochemical fabrication of sub-20 nm solid-state nanopores for single-molecule biosensing', *J. Phys. Condens. Matter*, 2010, **22**, (45), p. 454128
[21] Zhe J., Jagtiani A., Dutta P., *ET AL.*: 'A micromachined high throughput Coulter counter for bioparticle detection and counting', *J. Micromech. Microeng.*, 2007, **17**, (2), p. 304
[22] Kuo T.-C., Cannon D.M.J., Chen Y., *ET AL.*: 'Gateable nanofluidic interconnects for multilayered microfluidic separation systems', *Anal. Chem.*, 2003, **75**, (8), pp. 1861–1867
[23] de Jong J.: 'Application of membrane technology in microfluidic devices', University of Twente, 2008
[24] Guzel F.D., Citak F.: 'Development of an on-chip antibiotic permeability assay with single molecule detection capability', *IEEE Trans. Nanobiosc.*, 2018, **17**, (2), p. 1
[25] Holmes M.R., Shang T., Hawkins A.R., *ET AL.*: 'Micropore and nanopore fabrication in hollow antiresonant reflecting optical waveguides', *Journal of micro/nanolithography, MEMS, and MOEMS: JM3*, 2010, **9**, pp. 23004–23006
[26] Rudenko M.I., Holmes M.R., Ermolenko D.N., *ET AL.*: 'Controlled gating and electrical detection of single 50S ribosomal subunits through a solid-state nanopore in a microfluidic chip', *Biosens. Bioelectron.*, 2011, **29**, (1), pp. 34–39
[27] Gong X., Patil A. V, Ivanov A.P., *ET AL.*: 'Label-free in-flow detection of single DNA molecules using glass nanopipettes', *Anal. Chem.*, 2014, **86**, (1), pp. 835–841
[28] Streets A.M., Huang Y.: 'Microfluidics for biological measurements with single-molecule resolution', *Curr. Opin. Biotechnol.*, 2014, **25**, pp. 69–77
[29] Beamish E., Kwok H., Tabard-Cossa V., *ET AL.*: 'Precise control of the size and noise of solid-state nanopores using high electric fields', *Nanotechnology*, 2012, **23**, (40), p. 405301
[30] Schoch R.B., Han J., Renaud P.: 'Transport phenomena in nanofluidics', *Rev. Mod. Phys.*, 2008, **80**, (3), pp. 839–883
[31] Chen P., Gu J., Brandin E., *ET AL.*: 'Probing single DNA molecule transport using fabricated nanopores', *Nano Lett.*, 2004, **4**, (11), pp. 2293–2298
[32] Muthukumar M.: 'Translocation of a confined polymer through a hole', *Phys. Rev. Lett.*, 2001, **86**, (14), pp. 3188–3191
[33] Wanunu M., Morrison W., Rabin Y., *ET AL.*: 'Electrostatic focusing of unlabelled DNA into nanoscale pores using a salt gradient', *Nat. Nanotechnol.*, 2009, **5**, p. 160
[34] Stone H.A.: 'Introduction to fluid dynamics for microfluidic flows', in Lee H., Westervelt R.M., Ham D. (Eds.): 'CMOS biotechnology' (Springer, USA, 2007), pp. 5–30
[35] Stellwagen N.C., Gelfi C., Righetti P.G.: 'The free solution mobility of DNA', *Biopolym.*, 1997, **42**, (6), pp. 687–703
[36] Xie P., Xiong Q., Fang Y., *ET AL.*: 'Local electrical potential detection of DNA by nanowire–nanopore sensors', *Nat. Nanotechnol.*, 2011, **7**, p. 119
[37] Meller A., Branton D.: 'Single molecule measurements of DNA transport through a nanopore', *Electrophoresis*, 2002, **23**, (16), pp. 2583–2591
[38] Han J., Craighead H.G.: 'Separation of long DNA molecules in a microfabricated entropic trap array', *Science*, 2000, **288**, (5468), pp. 1026–1029
[39] Mohiuddin Mala G., Li D.: 'Flow characteristics of water in microtubes', *Int. J. Heat Fluid Flow*, 1999, **20**, (2), pp. 142–148

7. Appendix

7.1. Appendix 1: The capture of the molecule (e.g. DNA) by the nanopore is governed by two physical regimes; *diffusion-limited regime* where the molecule is far away from the pore mouth ($r^* < r$, the radial distance between the pore entrance and the position of the molecule in the cis chamber), and *energy barrier-limited regime* at a distance of $r^* \sim r$ [33]. Representative image of the capture can be found in Fig. 5*a*. In the diffusion-limited regime, the molecule diffuses randomly in the solution owing to the Brownian motion and its capture is limited by the time that the molecule travels to the pore mouth. When the molecule approaches to the pore, the effect of the electric field becomes more dominant compared to the diffusive forces, where the molecule entry to the pore is limited by an activation energy created by the electric field. Referring to an energy-barrier limited regime, mthe olecule no longer freely diffuses in this regime, rather is driven towards the nanopore by a space dependent drift velocity

$$v(h) = \mu_{\text{ep}} \nabla V(r) \tag{1}$$

where μ_{ep} is the electrophoretic mobility of molecule, and $V(r)$ is the potential at a distance of r from the pore, represented as

$$V(r) = \left(\frac{d_{\text{pore}}^2}{8 L_{\text{pore}} r}\right) \Delta V \tag{2}$$

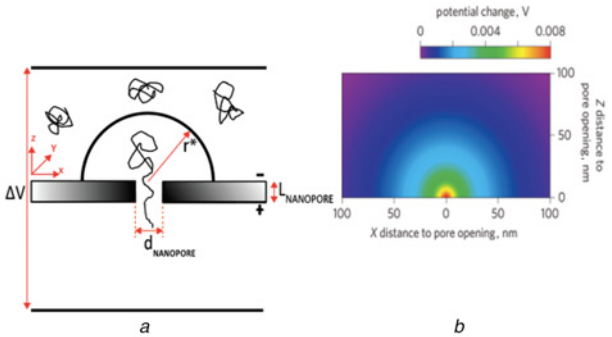

Fig. 5 *Schematic representations of DNA capture*
a Schematic diagram of DNA capture at the nanopore entrance upon the application of the certain potential, modified from [33]
b Simulated electric potential map of the trans side of a 10 nm nanopore during translocation at a potential of 1 V [36]

doi: 10.1049/mnl.2018.5206

where ΔV is the potential drop across the pore, d_{pore} is the nanopore diameter, and L_{pore} is the nanopore thickness. $V(r)$ defines the electric field profile in the system and is highly dependent on the nanopore geometry. Clearly, at close distance to the pore mouth ($r^* \sim r$), the electric field is relatively stronger (an example of the electric potential map on the trans side of the nanopore can be seen in Fig. 5*b*) and creates an electrophoretic trap for the negatively charged molecule. The electrophoretic trap is defined by a free energy barrier which includes entropic trapping effects and an enthalpy term covering specific and non-specific DNA–nanopore interactions as well as ions depletion from the pore due to DNA entry [37, 38].

The distance r^* can be estimated from the relationship between the electrophoretic speed (V_{ep}) and the diffusional speed of the molecule (V_{diff}) [33]. In particular, once the molecule approaches the pore, where the cross-over between $r^* < r$ and $r^* > r$ occurs, V_{diff} becomes comparable to V_{ep}. V_{diff} can be approximated from the diffusion time (t_{diff}) required for the molecule to travel from the distance r to the pore entrance

$$V_{diff} \sim \frac{r}{t_{diff}} \sim \frac{r}{r^2/D} \sim \frac{D}{r} \tag{3}$$

where D is the diffusion coefficient and t_{diff} is expressed by the Brownian motion. V_{ep} is defined by the following equation:

$$V_{ep} = -\mu_{ep} E(r) \tag{4}$$

where $E(r)$ is expressed as follows:

$$E(r) \cong \frac{V(r)}{r} \tag{5}$$

The relationship between V_{diff} and V_{ep}, based on the fact that V_{ep} is more pronounced than V_{diff} at a distance of $r^* > r$, leads to the expression of r^* as follows:

$$r^* \cong \frac{d_{pore}^2 \mu_{EP}}{8 L_{pore} D} \Delta V \tag{6}$$

where q is the charge of the molecule. The minus sign in (4) is used to represent the negative charge of DNA.

7.2. Appendix 2: From the simulations shown in Fig. 4*b* in the main text, it can be seen that the flow develops a continuous fashion at flow rates higher than 0.3 µl/min. $V(x)$ reaches a value of 3.5 and 133 mm/s at a flow rate of 30 µl/min at a distance of 500 nm away from the channel sides (namely nanopore capture zone) and at the centre of the channel, respectively, whereas it corresponds to a speed of <0.1 µm/s and ~1.5 µm/s at a flow rate of 0.3 µl/min, respectively. Nonetheless, Mohiuddin Mala and Li [39] reported that flow profile deviates from the expectations at high Reynolds number, thus high flow rates (e.g. $Re < 500$, corresponding to a fluid velocity of 83 mm/s). This means that the numbers given above might vary slightly for certain flow rates.